BBA - Molecular Basis of Disease 1865 (2019) 165523

Contents lists available at ScienceDirect

BBA - Molecular Basis of Disease

journal homepage: www.elsevier.com/locate/bbadis

IDH2 deficiency impairs cutaneous wound healing via ROS-dependent apoptosis

Sung Hwan Kim, Jeen-Woo Park*

School of Life Sciences and Biotechnology, BK21 Plus KNU Creative BioResearch Group, College of Natural Sciences, Kyungpook National University, Taegu, Republic of Korea

ARTICLE INFO

Keywords:
Wound healing
Apoptosis
IDH2
Mitochondria
Mito-TEMPO

ABSTRACT

Dermal fibroblasts are mesenchymal cells found between the skin epidermis and subcutaneous tissue that play a pivotal role in cutaneous wound healing by synthesizing fibronectin (a component of the extracellular matrix), secreting angiogenesis factors, and generating strong contractile forces. In wound healing, low concentrations of reactive oxygen species (ROS) are essential in combating invading microorganisms and in cell-survival signaling. However, excessive ROS production impairs fibroblasts. Mitochondrial $NADP^+$-dependent isocitrate dehydrogenase (IDH2) is a key enzyme that regulates the mitochondrial redox balance and reduces oxidative stress-induced cell injury through the generation of NADPH. In the present study, the downregulation of IDH2 expression resulted in an increase in cell apoptosis in mouse skin through ROS-dependent ATM-mediated p53 signaling. IDH2 deficiency also delayed cutaneous wound healing in mice and impaired dermal fibroblast function. Furthermore, pretreatment with the mitochondria-targeted antioxidant mito-TEMPO alleviated the apoptosis induced by IDH2 deficiency both in vitro and in vivo. Together, our findings highlight the role of IDH2 in cutaneous wound healing in association with mitochondrial ROS.

1. Introduction

Skin is a barrier system that protects the body from injuries, bacterial infiltration, and the loss of water. When the skin is injured, fibroblasts play a pivotal role in cutaneous wound healing by proliferating and migrating to the wound bed, where they produce extracellular matrix proteins, such as fibronectin, form granulation tissue, and generate strong contractile forces to draw the wound margins toward one another. When the wound has been replaced with a fibrotic scar, the fibroblasts are removed via apoptosis [1–3].

Reactive oxygen species (ROS) are generated by cellular metabolism, particularly within the mitochondria. Growing evidence suggests that ROS are crucial regulators of several phases of the healing process, with low concentrations of ROS necessary to repel invading microorganisms and involved in cell survival signaling [4]. In the early stages of wound healing, ROS initiate platelet aggregation and stimulate the diapedesis of adherent leukocytes across the blood vessel wall in order to kill microorganisms at the site of the injury. ROS also promote fibroblast proliferation and migration and mediate TGF-β1 signaling, which results in the production of fibronectin and the expression of growth factors [4,5]. In addition, ROS has been shown to stimulate angiogenesis, endothelial cell division and migration via VEGF expression, while also stimulating the proliferation and migration of fibroblasts, leading to the formation of the extracellular matrix (ECM). At the same time, keratinocyte proliferation and migration are promoted, facilitating re-epithelialization. However, excessive ROS production leads to oxidative stress that can, directly and indirectly, modify and degrade ECM proteins and also impair fibroblasts and keratinocytes [4].

Mitochondrial $NADP^+$-dependent isocitrate dehydrogenase (IDH2) controls the energy and redox status and catalyzes the oxidative decarboxylation of isocitrate to α-ketoglutarate, thus producing NADPH, a cofactor that is fundamental for the regeneration of the thioredoxin system [6] and for maintaining the pool of reduced glutathione (GSH). Glutathione reductase generates GSH via the NADPH-dependent recycling of oxidized glutathione (GSSG). When under oxidative stress, GSSG accumulates and alters the mitochondrial GSH to GSSG ratio, which serves as a marker for cellular oxidative stress [7]. Therefore, in providing NADPH for NADPH-dependent antioxidant enzymes, IDH2 plays an important role in regulating the mitochondrial redox balance and reducing oxidative stress-induced cell damage [8]. It has also been reported that IDH2-knockout mice develop heart failure, heart cell apoptosis, and hypertrophy [7]. IDH2 deficiency also induces endothelial dysfunction by causing dynamic mitochondrial changes and

* Corresponding author.
E-mail address: parkjw@knu.ac.kr (J.-W. Park).

https://doi.org/10.1016/j.bbadis.2019.07.017
Received 29 April 2019; Received in revised form 29 July 2019; Accepted 30 July 2019
Available online 31 July 2019
0925-4439/

impairing vascular function [9]. However, the effect of IDH2 on cutaneous wound healing has yet to be elucidated. With this in mind, we demonstrated that IDH2-deficient mice exhibit delayed cutaneous wound healing due to impaired dermal fibroblast function. In particular, IDH2 deficiency induced p53-mediated apoptosis through the modulation of ROS-dependent p53 signaling. This study confirmed that IDH2 plays an important role in wound healing.

2. Materials and methods

2.1. Animal preparation

Experiments were performed using 8-week-old male C57BL/6 mice, consisting of wild-type (WT) *Idh2*$^{+/+}$ and knockout (KO) *Idh2*$^{-/-}$ genotypes generated by breeding and identified by PCR genotyping, as previously described [10]. For mito-TEMPO experimentation, the mice received a daily injection of mito-TEMPO (0.7 mg/kg, intraperitoneal) starting at week 6 for 30 days. The mice were allowed free access to water and standard mouse chow. The temperature (23 ± 2 °C), humidity (50 ± 5%), and daily 12 h light–dark cycle was kept constant in the Central Laboratory Animal Facility at Kyungpook National University. All animal procedures were conducted in accordance with the Institutional Animal Care guidelines issued by the Committee of Animal Research at Kyungpook National University.

2.2. Primary cells culture

Primary dermal fibroblasts from wild-type (WT) *Idh2*$^{+/+}$ and knockout (KO) *Idh2*$^{-/-}$ mice were established via the enzymatic digestion of the dorsal dermal skin using collagenase I [11]. Primary murine dermal fibroblasts were maintained in DMEM/F12 containing 15% FBS and 1% of an antibiotic/antimycotic mixture in a humidified incubator at 37 °C and 5% CO_2.

2.3. Excisional wound preparation

The hair of the back of the mouse was shaved with electric clippers followed by the application of depilatory cream. To make an excisional wound, the skin was first rinsed with alcohol, and sterile skin biopsy punches (Miltex Inc., York, PA) with a diameter of 5 mm were then used to create four full-thickness skin wounds on the dorsal surface (back) of the mouse. Following this, the mice were caged individually, and the wounds were not dressed.

2.4. RNA isolation and reverse transcription (RT)-PCR

To extract mRNA, a piece of whole skin (1 cm × 1 cm) was treated with 500 μL of TRIzol reagent and incubated for 30 min at room temperature. RNA was reverse transcribed to cDNA using a First-Strand cDNA Synthesis Kit (Invitrogen) following the manufacturer's protocol. The cDNA was amplified using the polymerase chain reaction (PCR) method. The sequences of the primers used were as follows: *β-actin*, forward 5′-TCTACAATGAGCTGCGTGTG-3′, reverse 5′-ATCTCCTTCTG CATCCTGTC-3′; and *Idh2*, forward 5′-ATCAAGGAGAAGC-TCATCC TGC-3′, reverse 5′-TCTGTGGCCTTGTACTGGTCG-3′. β-Actin was used as an internal control. The amplified DNA products were resolved on 1% agarose gel and stained with ethidium bromide.

2.5. Immunofluorescence and histological analysis

The present study utilized the following commercial antibodies for immunofluorescence and histological analysis: TNF-α (11948) and vascular endothelial growth factor (SC-152) from Cell Signaling Technology (Beverly, MA); α-smooth muscle actin (α-SMA, ab5694), 8-hyroxy-2′-deoxyguanosine (8-OH-dG, ab62623), and Ki67 (ab16667) from Abcam (Cambridge, MA); NADPH (orb11152) from Biorbyt (Cambridge, UK); oxidized peroxiredoxin (Prx-SO_3, LF-PA0004) from AbFrontier (Seoul, Korea); IDH2 (SAB2501533) from Sigma Aldrich (St. Louis, MO); and HSP47 (SC-5293), phospho-p53 (SC-71786), fibronectin (SC-8422), collagen 6 (SC-377143), PECAM (SC-376764), and β-actin (SC-47778) from Santa Cruz Biotechnology (Santa Cruz, CA). Dermal fibroblasts were fixed with 3% formaldehyde in PBS for 15 min at room temperature and gently washed twice with PBS. Acetone permeabilization was performed with 100% ice-cold acetone at −20 °C for 10 min. After fixation, immunostaining was conducted as previously described [7]. Wound specimens were fixed in 4% formaldehyde and then embedded with paraffin, and 5-μm sections were sliced. Each slide was subjected to deparaffinization and rehydration, followed by antigen unmasking. The sections were boiled at 98 °C in a 10 mM sodium citrate buffer for 10 min and cooled for 20 min. Immunostaining was conducted as previously described [12]. To determine skin morphology, wound specimens were sequentially stained with hematoxylin Gill No. 3, bluing solution, and eosin Y via gentle shaking at room temperature. Connective tissue (i.e., dermis and hypodermis) regeneration in the wound was assessed following trichrome staining with a Masson trichrome staining kit. The collagen fibers of the connective tissue within the dermis and hypodermis were stained blue.

2.6. Immunoblot analysis

The following commercial antibodies were used for immunoblot analysis in the present study: VEGF (SC-152) (Cell Signaling Technology); phospho-Chk2 (ab59408), phospho-E2F1 (ab55325) and α-SMA (ab5694) (Abcam); Prx-SO_3 (LF-PA0004) (AbFrontier); IDH2 (SAB2501533) (Sigma Aldrich); and HSP47 (SC-5293), phospho-p53 (SC-71786), fibronectin (SC-8422), collagen 6 (SC-377143), PECAM (SC-376764), phospho-ATM (SC-47739), and β-actin (SC-47778). Conventional immunoblotting procedures were used to detect the target proteins. The cells were collected, washed once in cold PBS, and then scraped in a TEGN buffer (10 mM Tris, pH 8, 1 mM EDTA, 10% glycerol, 0.5% Nonidet P-40, 400 mM NaCl, 1 mM DTT, 0.5 mM phenylmethylsulfonylfluoride, and protease inhibitor mixture containing 1 M benzamidine, 3 mg/mL leupeptin, 100 mg/ mL bacitracin, and 1 mg/mL α2 macroglobulin) and incubated on ice for 15 min. Lysates were then cleared using centrifugation at 20,000*g* for 10 min. The total protein concentration was determined using Bio-Rad protein assays. Equal amounts of protein were separated on 10% SDS-PAGE and the proteins were transferred to nitrocellulose membranes (Bio-Rad). The membranes were then blocked for 1 h in a PBS solution containing 5% nonfat milk powder and 0.1% Tween-20 and then probed with primary antibodies overnight in 1% milk and 0.1% Tween-20 in PBS. After washing, the membranes were incubated for 1 h with a horseradish peroxidase-linked secondary antibody (Sigma Aldrich) in 1% milk and 0.1% Tween-20 in PBS. Finally, after three 5-min washes in 0.1% PBS/Tween-20, the proteins were visualized using enhanced chemiluminescence (Amersham Biosciences). Band intensities were quantified with ImageQuant 5.2 software.

2.7. In vitro cell migration assays

Scratch-wound assays were used to detect the migration of dermal fibroblasts in vitro as described previously [13]. Dermal fibroblasts were grown to 80–90% confluence in 12-well plates in serum-free DMEM/F12. The plates were mechanically scratched with a sterile 10-μl pipette tip to create two perpendicular linear lines. The cells were extensively rinsed with phosphate-buffered saline (PBS) to remove cellular debris. The progression of migration was photographed immediately and 30 h after wounding in the same field near the crossing point using a digital camera (Nikon) connected to a Zeiss Axiovert 200 inverted microscope. The degree of wound healing was determined by the distance traversed by the cells migrating into the denuded area. The horizontal lines indicated the wound edge. The migration of dermal

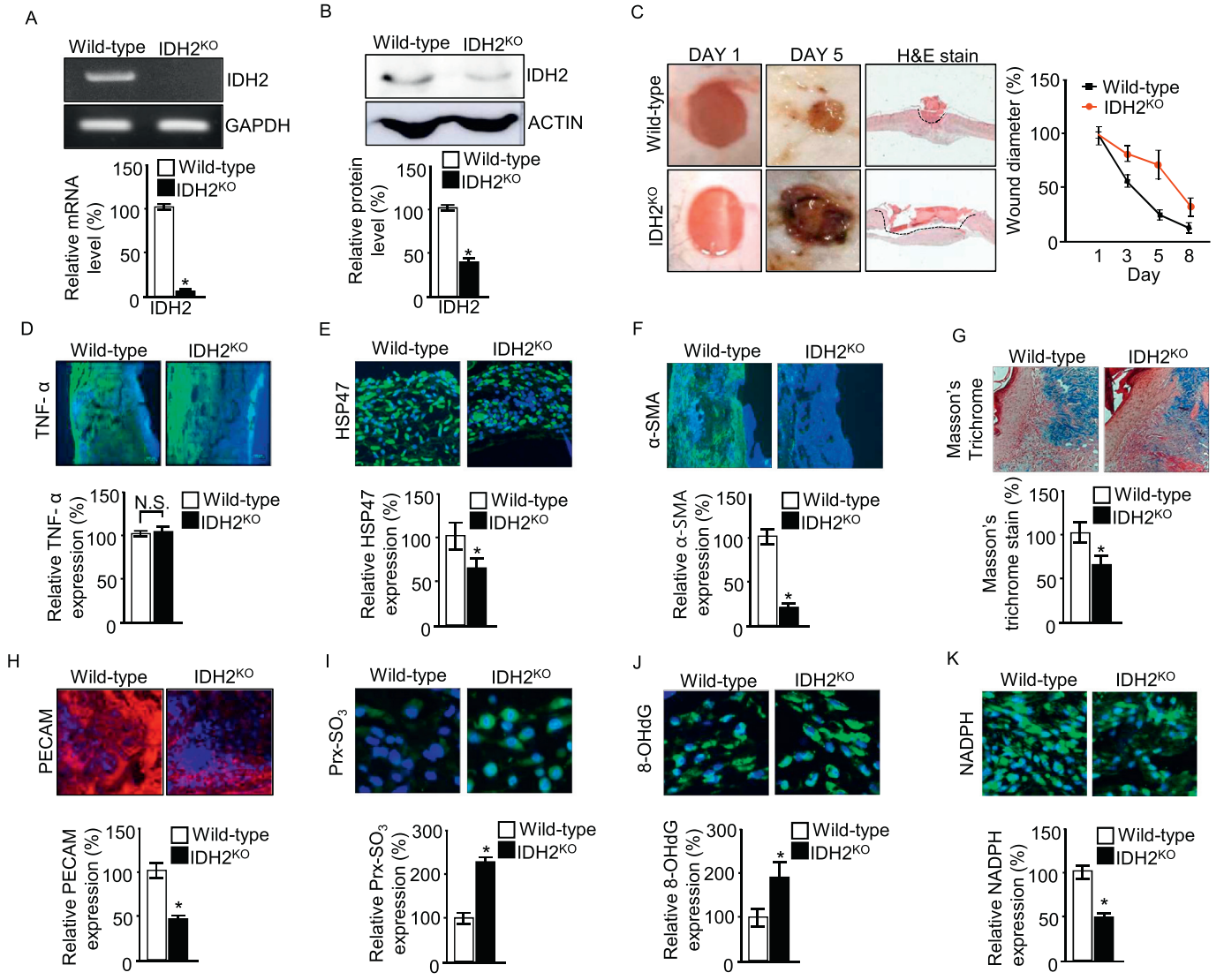

Fig. 1. Delayed wound healing in *Idh2*$^{-/-}$ KO mice. (A) RT-PCR analysis of IDH2 gene expression of skin from WT and *Idh2*$^{-/-}$ mice. β-Actin was used as an internal control. (B) Immunoblotting analysis of IDH2 protein expression in the skin of *Idh2*$^{+/+}$ and *Idh2*$^{-/-}$ mice. β-Actin was used as an internal control. (C) Macroscopic images and histological observations of wound healing on days 1 and 5 in wild-type (WT) *Idh2*$^{+/+}$ and knockout (KO) *Idh2*$^{-/-}$ mice. Cutaneous wounds (5 mm) were created on the backs of the mice and wound closure was monitored. Skin sections stained with H&E revealed wound histology on day 5 post-injury. (D-F) Immunofluorescence staining for TNF-α, HSP47, and α-SMA (all stained green) in skin tissues from *Idh2*$^{+/+}$ and *Idh2*$^{-/-}$ mice. The histograms represent the quantification of fluorescence intensity. (G) Masson-Trichrome staining of the reticular dermis of *Idh2*$^{+/+}$ and *Idh2*$^{-/-}$ mice shows differences in the collagen matrix architecture after full-thickness wound healing. (H–K) Immunofluorescence staining for PECAM (red), Prx-SO_3 (green), 8-OHdG (green) and NADPH (green) in skin tissue from *Idh2*$^{+/+}$ and *Idh2*$^{-/-}$ mice. The histograms represent the quantification of fluorescence intensity. In (B) and (C), each value represents the mean ± SD from three independent experiments. *$p < 0.05$ compared with the *Idh2*$^{+/+}$ mice group. The figures show representative data for three independent experiments. In D-K, the results are shown as the mean ± SD ($n = 6$ mice). *$p < 0.05$ between the two genotypes indicated. (For interpretation of the references to color in this figure legend, the reader is referred to the online version of this chapter.)

fibroblasts across the wound margins after 30 h was assessed and photographed using inverted microscopy. The recovered area width was calculated as the wound area width 30 h after injury subtracted from the original wound area width and expressed as a % of the control recovered area width. Recovered area width means that the dermal fibroblast migration distance or wound closure rate was (wound area at 0 h − wound area at 30 h) × 100/wound area at 0 h. Wound area widths were quantified with imageJ software.

2.8. Transwell invasion assays

Dermal fibroblasts were incubated in DMEM/F12 with 15% FBS and collected by trypsinization. A cell suspension (200 μL of 5 × 10^5 cells/ml with 1% FBS) was added into the inner cup of a 24-well Transwell chamber that had been coated with 50 μl of Matrigel™ (BD Biosciences; 1:4 dilution in serum-free medium). The medium, supplemented with 15% serum, was added to the outer cup. After 24 h, non-invading cells were removed from the upper surface by gently rubbing with a cotton-tipped swab. Cells that had migrated through the Matrigel and the 8-μm pore membrane were fixed with 3% paraformaldehyde for 20 min, stained with crystal violet for 25 min and then counted in five random microscopic fields on the lower filter surface. Each experiment was performed in triplicate [14].

2.9. Collagen contraction assays

After 5 days of TGF-β1 treatment, wild-type (WT) *Idh2*$^{+/+}$ and knockout (KO) *Idh2*$^{-/-}$ dermal fibroblasts were plated at densities of

6×10^5 cells/well and seeded into wells, each containing 0.5 ml of collagen gel lattice (Biolabs, San Diego, CA). After polymerization, 1 ml of culture medium was added. After two days of culturing, stressed matrices were released from the surrounding brims of the wells using a sterile pipette tip. Images of the free-floating collagen gel lattices were taken immediately after the release of the gel (0 h) and at 72 h. Areas of collagen gel size were analyzed using ImageJ (National Institutes of Health, Bethesda, MD). The degree of contraction was calculated by determining the area of the gel matrix.

2.10. Terminal deoxynucleotidyl transferase-mediated dUTP nick-end labeling (TUNEL) staining

TUNEL staining was employed to evaluate cell apoptosis in the mouse skin sections and dermal fibroblasts using the In-Situ Cell Death Detection Kit (Roche, Basel, Switzerland) according to the manufacturer's recommended protocol. TUNEL-stained slides were lightly counterstained with 4′,6-diamidino-2-phenylindole (DAPI) before final mounting. The stained slides were analyzed under an Axiovert 40 CFL microscope (Carl Zeiss AG; Oberkochen, Germany).

2.11. Determination of mitochondrial ROS levels

MitoSOX-red (Molecular Probes, Eugene, OR, USA) is a fluorogenic indicator of superoxide generated specifically by mitochondria [15]. Dermal fibroblasts were washed with PBS and stained with 5 μM MitoSOX-red for 30 min in a humidified atmosphere of 5% CO_2 at 37 °C. After washing with PBS, the specimens were visualized using a Zeiss Axio Imager A2 fluorescence microscope (Carl Zeiss, Oberkochen, Germany).

2.12. Statistical analyses

Statistical analysis was conducted using 2-tailed Student's *t*-tests, with $p < 0.05$ considered statistically significant. The data were analyzed by comparing treated and untreated contralateral structures or by comparing treated and control mice.

3. Results and discussion

3.1. IDH2 deficiency impaired wound healing

We confirmed the loss of *Idh2* gene expression and IDH2 protein expression in the skin of knockout (KO) *Idh2*$^{-/-}$ mice using RT-PCR and Western blot analysis of whole-skin lysates (Fig. 1A and B). To identify the functional effect of IDH2 in cutaneous wound healing, we established a full-thickness excision mice model. Wounds were made on the skin of the backs of the mice using a 5-mm biopsy punch, and the healing process was observed for 8 days. Throughout the healing process, a more significant delay was observed 5 days after wounding in the *Idh2*$^{-/-}$ mice compared to the *Idh2*$^{+/+}$ mice (Fig. 1C).

Wound healing involves a series of consecutive and overlapping phases consisting of inflammation, the formation of granulation tissue including fibroblast accumulation, myofibroblast differentiation, angiogenesis, extracellular matrix synthesis, re-epithelialization, and tissue remodeling. To explore the possible mechanisms involved in delayed wound healing in *Idh2*$^{-/-}$ mice, skin tissue was analyzed using immunohistochemistry 5 days after wounding. In order to determine differences in the inflammation reaction, we used immunofluorescence staining to examine the levels of cytokine protein TNF-α, which is involved in systemic inflammation. Immunofluorescence staining revealed no significant changes in TNF-α protein levels in *Idh2*$^{+/+}$ mice and *Idh2*$^{-/-}$ mice (Fig. 1D). However, the number of dermal fibroblasts in the skin of *Idh2*$^{-/-}$ mice was lower than in *Idh2*$^{+/+}$ mice (Fig. 1E). Myofibroblast differentiation, collagen deposition, and angiogenesis were also inhibited in *Idh2*$^{-/-}$ mice to a greater extent than in *Idh2*$^{+/+}$ mice (Fig. 1F–H). In order to determine changes of redox status, we used immunofluorescence staining to examine the levels of oxidized peroxiredoxin (Prx-SO_3) and 8-OHdG, which is a marker for intracellular ROS formation and oxidative DNA damage. Oxidative stress was higher in the skin of *Idh2*$^{-/-}$ mice than in that of *Idh2*$^{+/+}$ mice (Fig. 1I and J). In addition, NADPH levels were significantly more attenuated in *Idh2*$^{-/-}$ mouse skin than in *Idh2*$^{+/+}$ mouse skin (Fig. 1K). Excessive production of ROS or impaired ROS detoxification causes oxidative damage, which is the main cause of chronic non-healing wounds. Taking these results together, we hypothesize that the delayed wound healing in IDH2-deficient mice is due to the inhibition of fibroblast function by the increased levels of ROS.

3.2. IDH2 deficiency suppresses dermal fibroblast proliferation, migration, and invasion

Dermal fibroblasts are the most abundant cells in the skin. When a wound occurs, they begin to proliferate and migrate to the wound site, producing the ECM, initiating angiogenesis, and differentiating into myofibroblasts to generate strong contractile forces that draw the wound margins toward each other. To determine the functional differences of fibroblasts in IDH2-deficient mouse skin, we isolated primary dermal fibroblasts from *Idh2*$^{+/+}$ and *Idh2*$^{-/-}$ mice. As expected, cytosolic and mitochondrial ROS levels were significantly higher in *Idh2*$^{-/-}$ dermal fibroblasts than in those of *Idh2*$^{+/+}$ (Fig. 2A–C). In addition, oxidative DNA damage was higher in *Idh2*$^{-/-}$dermal fibroblasts than in *Idh2*$^{+/+}$ dermal fibroblasts (Fig. 2D). As shown in Fig. 2E, IDH2 deficiency increased the phosphorylation of p53, E2F1, Chk2 kinase, and ATM, which suggests that the activation of p53 and E2F1 contributed, at least in part, to IDH2-deficiency-induced p53-dependent apoptosis. Similar to the previous results, the phosphorylation of p53 and TUNEL-stained cells were more commonly observed in *Idh2*$^{-/-}$ dermal fibroblasts than in *Idh2*$^{+/+}$ dermal fibroblasts (Fig. 2F and G). We also found that proliferation, migration, and invasion was lower in *Idh2*$^{-/-}$ dermal fibroblasts than in *Idh2*$^{+/+}$ dermal fibroblasts (Fig. 2H–J). Collectively, our results indicate that IDH2 deficiency suppresses proliferation, migration, and invasion via the ROS-mediated activation of p53-dependent apoptosis.

3.3. IDH2 deficiency inhibits myofibroblast differentiation, angiogenesis, and ECM production

Many p53-regulated genes are implicated in cell morphology and movement, including those encoding α-SMA [16], VEGF [17], and fibronectin [18]. It has been reported that inducing the expression of p53 was accompanied by a significant decrease in the extracellular matrix (i.e., fibronectin) and a reduction in matrix fibrils, a decrease in the number and size of focal contacts, a smaller cell area, the establishment of more elongated cells, and changes to the actin cytoskeleton, such as the actin bundles becoming thinner and their number and size decreasing [16]. It is known that TGF-β1 is an important profibrotic cytokine closely related to the activation and differentiation of fibroblasts [19]. Hence, we examined the effects of IDH2 deficiency on myofibroblast differentiation following TGF-β1 treatment. Myofibroblasts are generally identified by their expression of α-SMA. As seen in Fig. 3A, we found that the levels of α-SMA were lower in TGF-β1-treated *Idh2*$^{-/-}$ dermal fibroblasts than in *Idh2*$^{+/+}$ dermal fibroblasts. Collagen type I gel contraction assays were then conducted to evaluate whether IDH2 deficiency blocks TGF-β1-induced contraction activity. In agreement with the data in Fig. 3A, we also found a significant reduction in the contraction activity of TGFβ1-treated *Idh2*$^{-/-}$ dermal fibroblasts when compared to *Idh2*$^{+/+}$ dermal fibroblasts.

Neovascularization is an important process for the maintenance of wound healing, in which fibroblasts play an important paracrine role. Members of the VEGF family include VEGF-A, -B, -C and -D, which are produced by normal human fibroblasts and are important in regulating

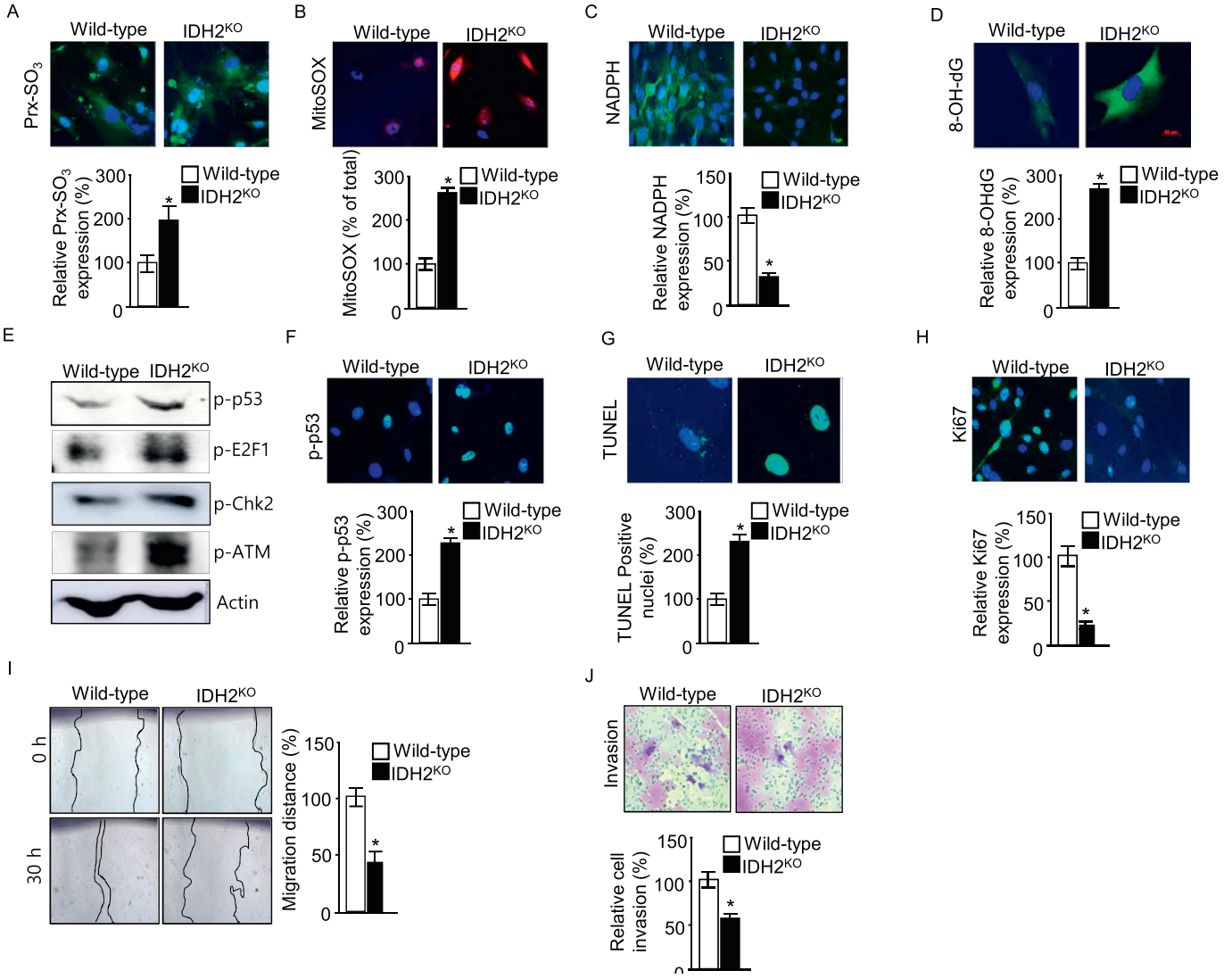

Fig. 2. Proliferation, migration, and invasion were repressed in *Idh2*$^{-/-}$ KO dermal fibroblasts. Primary murine dermal fibroblasts were isolated from WT and *Idh2*$^{-/-}$ mouse dorsal skin. (A) Representative immunofluorescence staining of Prx-SO_3 in dermal fibroblasts. The nuclei were counterstained with DAPI. The histograms represent the fluorescence intensity. (B) MitoSOX fluorescence levels for the assessment of mitochondrial ROS generation in *Idh2*$^{-/-}$ dermal fibroblast cells. The nuclei were counterstained with DAPI. The histograms represent the fluorescence intensity. (C) Representative immunofluorescence staining of NADPH (green) in dermal fibroblast cells. The nuclei were counterstained with DAPI. The histograms represent the fluorescence intensity. (D) Immunofluorescence image of oxidative DNA damage markers such as 8-OH-dG in dermal fibroblasts. The nuclei were counterstained with DAPI. The histograms represent the fluorescence intensity. (E) Immunoblot analysis of proteins related to ATM-mediated E2F1 activation in *Idh2*$^{-/-}$ dermal fibroblasts. β-Actin was used as an internal control. (F) Immunofluorescence microscopy image of pro-apoptotic markers such as phospho-p53 in dermal fibroblasts. The nuclei were counterstained with DAPI. The histograms represent the fluorescence intensity. (G) For quantification, apoptotic cells were stained using TUNEL assays. (H) Immunofluorescence microscopy image of proliferation markers such as Ki67 in dermal fibroblasts. The nuclei were counterstained with DAPI. The histograms represent the fluorescence intensity. (I) Representative images of the migration of WT and *Idh2*$^{-/-}$ dermal fibroblasts cultured for 30 h. The cell migration distance was calculated as described in the Materials and methods section. Changes in the transmigration distance were represented as a percentage of the control group. (J) Transwell invasion assays were used to evaluate the effect of IDH2 deficiency on dermal fibroblast cells invasion. Representative images of the invasion of WT and *Idh2*$^{-/-}$ dermal fibroblast cells through Matrigel ($n = 3$). Each value represents the mean ± SD from three independent experiments. *$p < 0.05$ compared with WT dermal fibroblast cells. The figures show representative data for three independent experiments. (For interpretation of the references to color in this figure legend, the reader is referred to the online version of this chapter.)

vascular cell proliferation through specific receptors [20]. It is also known that p53 inhibits VEGF expression by downregulating the transcriptional activity of Sp1 [17]. To determine whether the upregulation of p53 can inhibit VEGF expression in *Idh2*$^{-/-}$ dermal fibroblasts compared to *Idh2*$^{+/+}$ dermal fibroblasts, we conducted immunofluorescence microscopy analysis. As shown in Fig. 3C, we observed a reduction in VEGF expression in *Idh2*$^{-/-}$ dermal fibroblasts compared to *Idh2*$^{+/+}$ dermal fibroblasts.

In wound healing, fibronectin plays a critical role in ECM organization and stability. In vitro studies have revealed that fibronectin is required for the deposition of collagen I and other structural proteins in the ECM [21], and it is involved in cell adhesion and motility [22,23]. It is also known that p53 downregulates fibronectin gene expression [18]. We found that the expression of fibronectin was lower in *Idh2*$^{-/-}$ dermal fibroblasts than in *Idh2*$^{+/+}$ dermal fibroblasts (Fig. 3D). Thus, our findings suggest that IDH2 deficiency inhibits fibroblast differentiation, the secretion of angiogenesis-related factors, and ECM production.

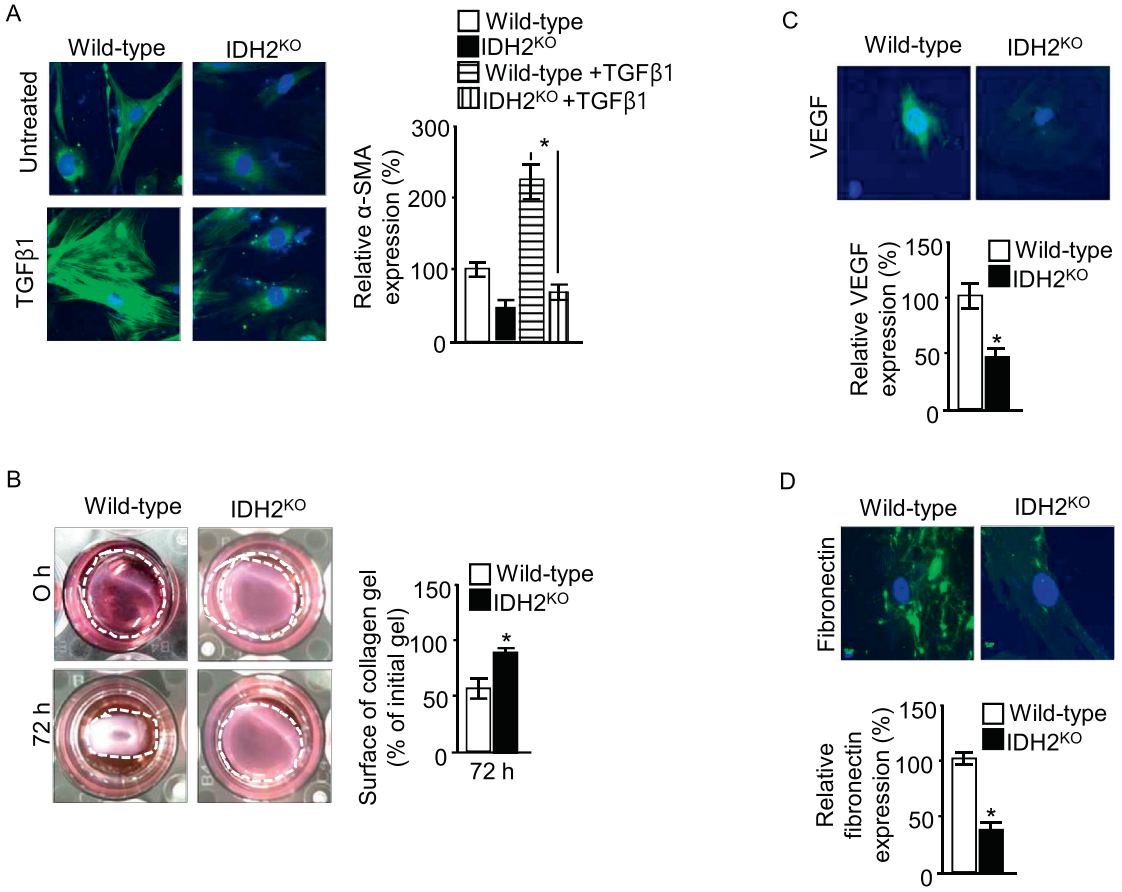

Fig. 3. IDH2 deficiency reduces myofibroblast differentiation and produces angiogenesis factors and ECM proteins. (A) Immunofluorescence staining of α-SMA (green) in WT and *Idh2*$^{-/-}$ dermal fibroblasts. The nuclei were counterstained with DAPI. The histograms represent the fluorescence intensity. (B) Serum-starved WT and *Idh2*$^{-/-}$ dermal fibroblasts treated with TGF-β1 (10 ng/ml) and collagen-gel contraction assays at 37 °C, and 5% CO_2 for 72 h. Representative digital images are presented. Representative images (left) and quantitation (right) are shown (*$p < 0.05$). In A and B, each value represents the mean ± SD from three independent experiments. *$p < 0.05$ against TGF-β1-treated WT dermal fibroblast cells. The figures present representative data for three independent experiments. In C and D, representative immunofluorescence staining of VEGF (green) and fibronectin (green) in WT and *Idh2*$^{-/-}$ dermal fibroblasts. The histograms represent the fluorescence intensity. Each value represents the mean ± SD from three independent experiments. *$p < 0.05$ against WT dermal fibroblast cells. The figures show representative data for three independent experiments. (For interpretation of the references to color in this figure legend, the reader is referred to the online version of this chapter.)

3.4. Mito-TEMPO protects against ROS-induced apoptosis in Idh2$^{-/-}$ *mouse skin and Idh2*$^{-/-}$ *dermal fibroblasts*

Our in vivo and in vitro experiments demonstrated that the impaired wound healing demonstrated in *Idh2*$^{-/-}$ mouse skin was the result of the accumulation of excessive ROS, leading to the apoptosis of dermal fibroblasts. Because IDH2 is a major NADPH-producing enzyme in the mitochondrial redox system, we hypothesized that the administration of effective mitochondrial antioxidants might promote the recovery of dermal fibroblast cells from ROS-induced apoptosis in *Idh2*$^{-/-}$ mouse skin. To determine whether mitochondrial ROS play a major role in impaired wound healing in response to IDH2 deficiency, mito-TEMPO, a novel mitochondria-targeted antioxidant that protects mitochondria from various forms of oxidative stress within a diverse range of pathological processes, was used [24,25]. First, the protective role of mito-TEMPO was evaluated in vivo. Male *Idh2*$^{-/-}$ mice (7-weeks old) received a daily intraperitoneal injection of mito-TEMPO (0.7 mg/kg) or a vehicle for 8 days. Wounds were made on the skin on the backs of the mice using a 5-mm biopsy punch, and the healing process was observed for 8 days. During the healing process, greater recovery was observed 5 days after wounding in the mito-TEMPO-treated *Idh2*$^{-/-}$ mice compared to the vehicle *Idh2*$^{-/-}$ mice (Fig. 4A).

Following this, to determine whether mito-TEMPO led to the recovery of dermal fibroblast function, we conducted migration assays and immunofluorescence microscopy analysis. As shown in Fig. 4B, *Idh2*$^{-/-}$ dermal fibroblasts exhibited inhibited migration while greater migration was observed in mito-TEMPO-treated *Idh2*$^{-/-}$ dermal fibroblasts. Additionally, to determine the effect of mito-TEMPO treatment on oxidative stress in response to IDH2 deficiency, immunofluorescence staining of Prx-SO_3 and mitoSOX was performed (Fig. 4C). We found a decrease in the intensity of Prx-SO_3 and mitoSOX in mito-TEMPO-treated *Idh2*$^{-/-}$ dermal fibroblasts compared to vehicle *Idh2*$^{-/-}$ dermal fibroblasts (Fig. 4C). Thus, treatment with mito-TEMPO resulted in the reduction of ROS levels, which have been shown to be higher in *Idh2*$^{-/-}$ dermal fibroblasts in vitro.

We also analyzed the activation of p53 with immunofluorescence staining to determine whether IDH2 deficiency affects the phosphorylation levels of p53 and the effect of mito-TEMPO treatment on apoptosis (Fig. 4D). The results show that the activation of p53 and apoptosis were lower in mito-TEMPO-treated *Idh2*$^{-/-}$ dermal fibroblasts compared with *Idh2*$^{-/-}$ dermal fibroblasts. To investigate the effect of mito-TEMPO treatment on the proliferation of IDH2-deficient cells, the immunocytochemistry of Ki67 was analyzed. As shown in Fig. 4E, mito-TEMPO treatment abrogated the decrease in the intensity of Ki67 and recovered Ki67 levels in *Idh2*$^{-/-}$ dermal fibroblasts. In addition, to determine the effect of mito-TEMPO treatment on differentiation and ECM production in response to IDH2 deficiency, immunofluorescence staining of α-SMA and fibronectin was conducted.

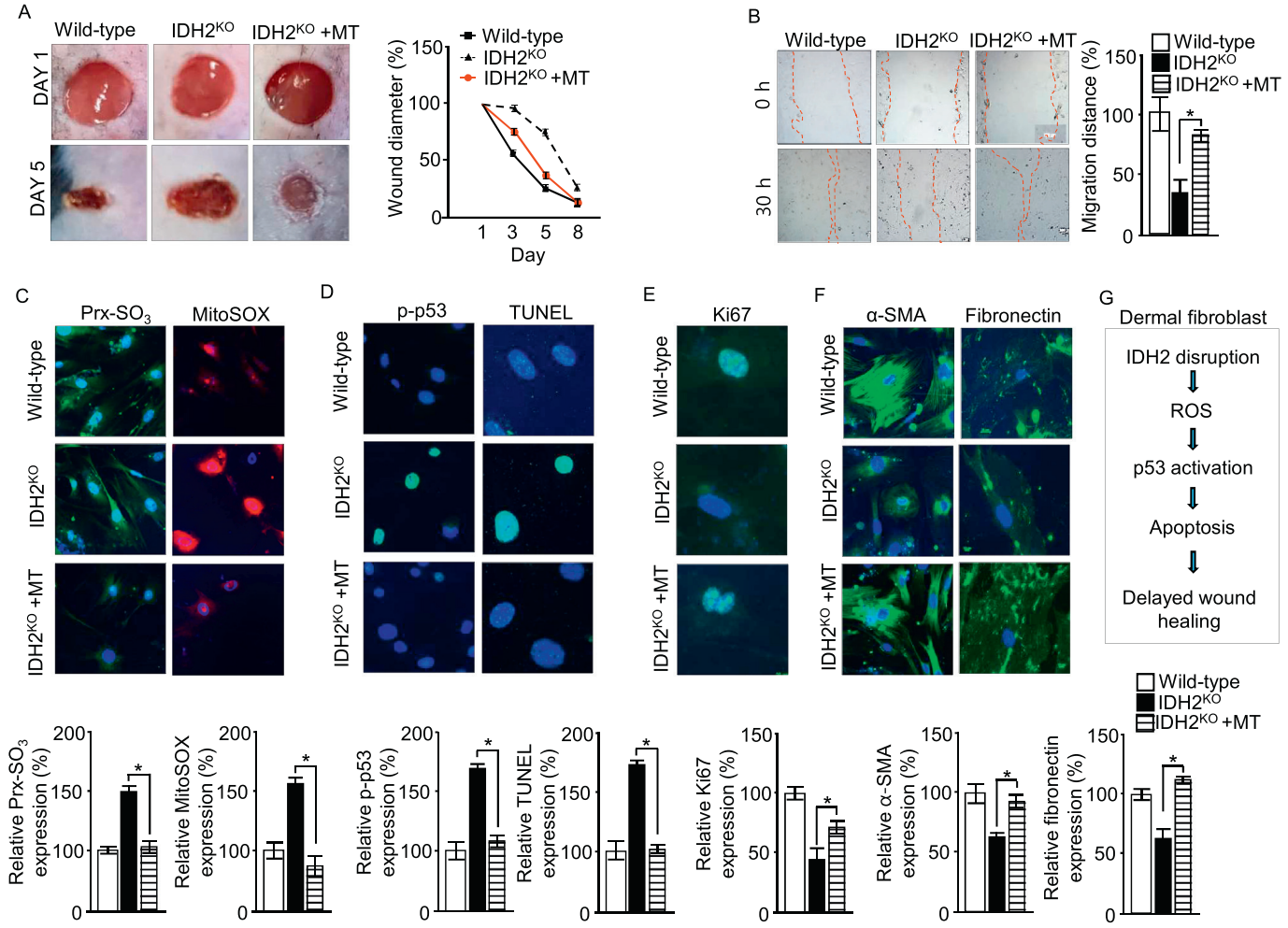

Fig. 4. Evaluation of the recovery effect of mito-TEMPO on delayed wound healing in *Idh2*$^{-/-}$ mice. (A) Macroscopic photographs and histological observations of wound healing on days 1 and 5 in WT, *Idh2*$^{-/-}$, and mito-TEMPO-treated *Idh2*$^{-/-}$ mice. Cutaneous wounds (5 mm) were created on the backs of mice and wound closure was monitored. (B) Representative images of the migration of WT, *Idh2*$^{-/-}$, and mito-TEMPO-treated *Idh2*$^{-/-}$ dermal fibroblasts cultured for 30 h. The cell migration distance was calculated as described in the Materials and methods section. Changes in the transmigration distance are represented as a percentage of the control group. (C) Representative immunofluorescence staining of Prx-SO_3 in WT, *Idh2*$^{-/-}$ and mito-TEMPO-treated *Idh2*$^{-/-}$ dermal fibroblasts. MitoSOX fluorescence level for the assessment of mitochondrial ROS generation in WT, *Idh2*$^{-/-}$, and mito-TEMPO-treated *Idh2*$^{-/-}$ dermal fibroblasts. (D) Immunofluorescence microscopy image of pro-apoptotic markers such as phospho-p53 in WT, *Idh2*$^{-/-}$, and mito-TEMPO-treated *Idh2*$^{-/-}$ dermal fibroblasts. Analysis of apoptosis by TUNEL staining in mito-TEMPO-treated *Idh2*$^{-/-}$ dermal fibroblasts compared with *Idh2*$^{-/-}$ dermal fibroblasts. (E) Immunofluorescence microscopy image of proliferation markers such as Ki67 in WT, *Idh2*$^{-/-}$, and mito-TEMPO-treated *Idh2*$^{-/-}$ dermal fibroblasts. (F) Immunofluorescence microscopy image of myofibroblast markers (α-SMA) and ECM proteins (fibronectin) in WT, *Idh2*$^{-/-}$, and mito-TEMPO-treated *Idh2*$^{-/-}$ dermal fibroblasts. (G) Schematic diagram summarizing IDH2-deficiency-induced delayed wound healing. In C–F, the nuclei were counterstained with DAPI. The histograms represent the fluorescence intensity. Each value represents the mean ± SD from three independent experiments. *$p < 0.05$ compared with WT dermal fibroblast cells. The figures show representative data for three independent experiments.

We found an increase in the intensity of α-SMA and fibronectin in mito-TEMPO-treated *Idh2*$^{-/-}$ dermal fibroblasts compared to vehicle *Idh2*$^{-/-}$ dermal fibroblasts (Fig. 4F).

In conclusion, the present study shows that IDH2 deficiency leads to increased oxidative stress and enhances apoptosis in dermal fibroblasts by disrupting the mitochondrial redox balance. Furthermore, our study provides a useful model for the investigation of the potential application of mito-TEMPO in the treatment or prevention of wound repair by regulating the mitochondrial redox balance. Overall, the impaired cutaneous wound healing observed in *Idh2*$^{-/-}$ mouse skin was linked to several factors that increase fibroblast apoptosis, including the enhanced ROS-mediated p53 signaling pathway (Fig. 4G). These results provide strong evidence further supporting the importance of mitochondrial redox balance in the regulation of wound healing.

Transparency document

The Transparency document associated with this article can be found, in online version.

Acknowledgments

This work was supported by the National Research Foundation of Korea (NRF) grants funded by the Korea government (MSIP) (2015R1A4A1042271 and 2019R1A2C1006125).

References

[1] V.A. Polunovsky, B. Chen, C. Henke, D. Snover, C. Wendt, D.H. Ingbar, P.B. Bitterman, Role of mesenchymal cell death in lung remodeling after injury, J. Clin. Invest. 92 (1993) 388–397.
[2] P. Martin, Wound healing–aiming for perfect skin regeneration, Science 276 (1997)

75–81.
[3] A. Desmouliere, C. Badid, M.L. Bochaton-Piallat, G. Gabbiani, Apoptosis during wound healing, fibrocontractive diseases and vascular wall injury, Int. J. Biochem. Cell Biol. 29 (1997) 19–30.
[4] M.H. Hoffmann, H.R. Griffiths, The dual role of Reactive Oxygen Species in autoimmune and inflammatory diseases: evidence from preclinical models, Free Radic. Biol. Med. 125 (2018) 62–71.
[5] D. Levigne, A. Modarressi, K.H. Krause, B. Pittet-Cuenod, NADPH oxidase 4 deficiency leads to impaired wound repair and reduced dityrosine-crosslinking, but does not affect myofibroblast formation, Free Radic. Biol. Med. 96 (2016) 374–384.
[6] Z.J. Reitman, H. Yan, Isocitrate dehydrogenase 1 and 2 mutations in cancer: alterations at a crossroads of cellular metabolism, J. Nat. Cancer Inst. 102 (2010) 932–941.
[7] H.J. Ku, Y. Ahn, J.H. Lee, K.M. Park, J.-W. Park, IDH2 deficiency promotes mitochondrial dysfunction and cardiac hypertrophy in mice, Free Radic. Biol. Med. 80 (2015) 84–92.
[8] S.Y. Park, S.M. Lee, S.W. Shin, S. W, J.-W. Park, Inactivation of mitochondrial NADP+-dependent isocitrate dehydrogenase by hypochlorous acid, Free Rad. Res. 42 (2008) 467–473.
[9] J.B. Park, H. Nagar, S. Choi, S.B. Jung, H.W. Kim, S.K. Kang, J.W. Lee, J.H. Lee, J.-W. Park, K. Irani, B.H. Jeon, H.J. Song, C.S. Kim, IDH2 deficiency impairs mitochondrial function in endothelial cells and endothelium-dependent vasomotor function, Free Radic. Biol. Med. 94 (2016) 36–46.
[10] S. Kim, S.Y. Kim, H.J. Ku, Y.H. Jeon, H.W. Lee, J. Lee, T.K. Kwon, K.M. Park, J.-W. Park, Suppression of tumorigenesis in mitochondrial NADP(+)-dependent isocitrate dehydrogenase knock-out mice, Biochim. Biophys. Acta 1842 (2014) 135–143.
[11] A. Seluanov, A. Vaidya, V. Gorbunova, Establishing primary adult fibroblast cultures from rodents, J. Vis. Exp. (44) (2010) e2033.
[12] S.H. Kim, H. Kim, H.J. Ku, J.H. Park, H. Cha, S. Lee, J.H. Lee, J.-W. Park, Oxalomalate reduces expression and secretion of vascular endothelial growth factor in the retinal pigment epithelium and inhibits angiogenesis: implications for age-related macular degeneration, Redox Biol. 10 (2016) 211–220.
[13] H. Izuta, Y. Chikaraishi, M. Shimazawa, S. Mishima, H. Hara, 10-Hydroxy-2-decenoic acid, a major fatty acid from royal jelly, inhibits VEGF-induced angiogenesis in human umbilical vein endothelial cells, Evid. Based Complement. Alternat. Med. 6 (2009) 489–494.
[14] D. Machado, S.M. Shishido, K.C. Queiroz, D.N. Oliveira, A.L. Faria, R.R. Catharino, C.A. Spek, C.V. Ferreira, Irradiated riboflavin diminishes the aggressiveness of melanoma in vitro and in vivo, PLoS One 8 (2013) e54269.
[15] K.M. Robinson, M.S. Janes, M. Pehar, J.S. Monette, M.F. Ross, T.M. Hagen, M.P. Murphy, J.S. Beckman, Selective fluorescent imaging of superoxide in vivo using ethidium-based probes, Proc. Natl. Acad. Sci. U. S. A. 103 (2006) 15038–15043.
[16] A. Alexandrova, A. Ivanov, P. Chumakov, B. Kopnin, J. Vasiliev, Changes in p53 expression in mouse fibroblasts can modify motility and extracellular matrix organization, Oncogene 19 (2000) 5826–5830.
[17] S. Pal, K. Datta, D. Mukhopadhyay, Central role of p53 on regulation of vascular permeability factor/vascular endothelial growth factor (VPF/VEGF) expression in mammary carcinoma, Cancer Res. 61 (2001) 6952–6957.
[18] V. Iotsova, D. Stehelin, Down-regulation of fibronectin gene expression by the p53 tumor suppressor protein, Cell Growth Differ. 7 (1996) 629–634.
[19] A.C. Midgley, M. Rogers, M.B. Hallett, A. Clayton, T. Bowen, A.O. Phillips, R. Steadman, Transforming growth factor-beta1 (TGF-beta1)-stimulated fibroblast to myofibroblast differentiation is mediated by hyaluronan (HA)-facilitated epidermal growth factor receptor (EGFR) and CD44 co-localization in lipid rafts, J. Biol. Chem. 288 (2013) 14824–14838.
[20] S. Trompezinski, O. Berthier-Vergnes, A. Denis, D. Schmitt, J. Viac, Comparative expression of vascular endothelial growth factor family members, VEGF-B, -C and -D, by normal human keratinocytes and fibroblasts, Exp. Dermatol. 13 (2004) 98–105.
[21] J. Sottile, D.C. Hocking, Fibronectin polymerization regulates the composition and stability of extracellular matrix fibrils and cell-matrix adhesions, Mol. Biol. Cell 13 (2002) 3546–3559.
[22] E. Ruoslahti, Fibronectin and its receptors, Annu. Rev. Biochem. 57 (1988) 375–413.
[23] A.R. Kornblihtt, A. Gutman, Molecular biology of the extracellular matrix proteins, Biol. Rev. Camb. Philos. Soc. 63 (1988) 465–507.
[24] A.E. Dikalova, A.T. Bikineyeva, K. Budzyn, R.R. Nazarewicz, L. McCann, W. Lewis, D.G. Harrison, S.I. Dikalov, Therapeutic targeting of mitochondrial superoxide in hypertension, Cir. Res. 107 (2010) 106–116.
[25] H.L. Liang, F. Sedlic, Z. Bosnjak, V. Nilakantan, SOD1 and MitoTEMPO partially prevent mitochondrial permeability transition pore opening, necrosis, and mitochondrial apoptosis after ATP depletion recovery, Free Radic. Biol. Med. 49 (2010) 1550–1560.